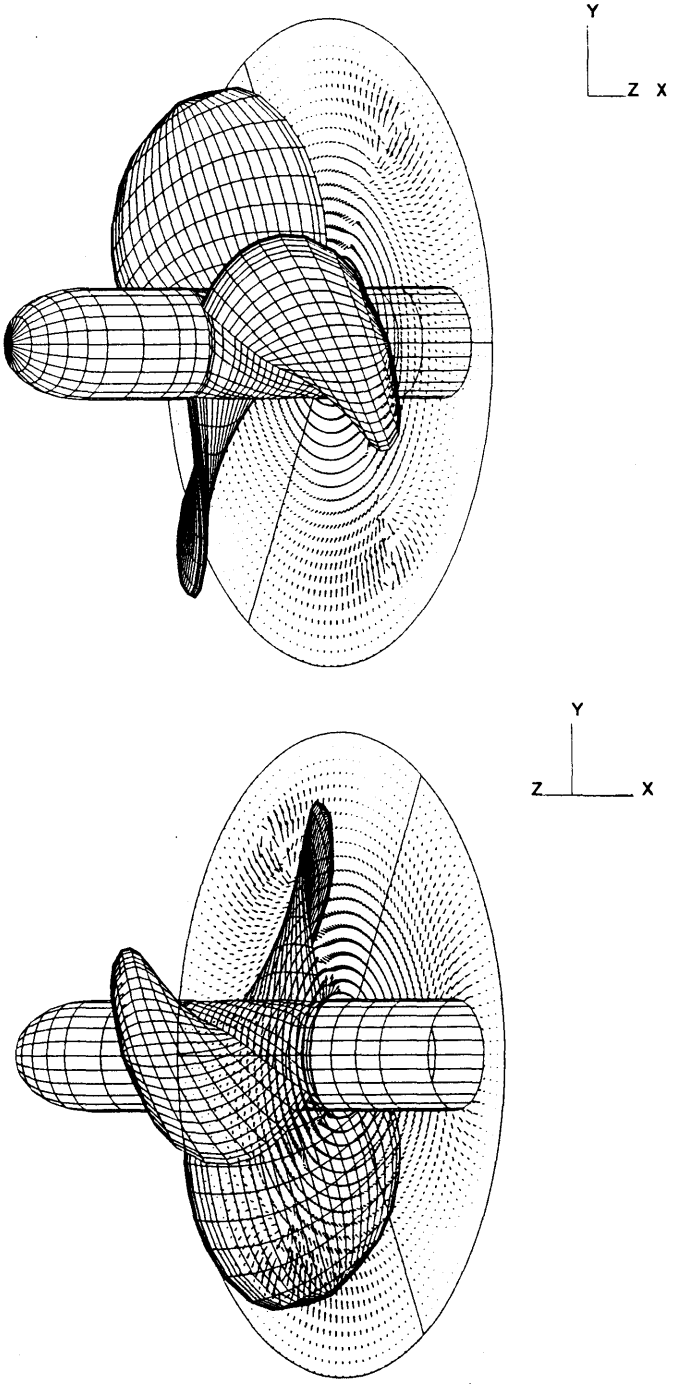

Fig. 1. Perspective Views of Discretized Propeller 4119.

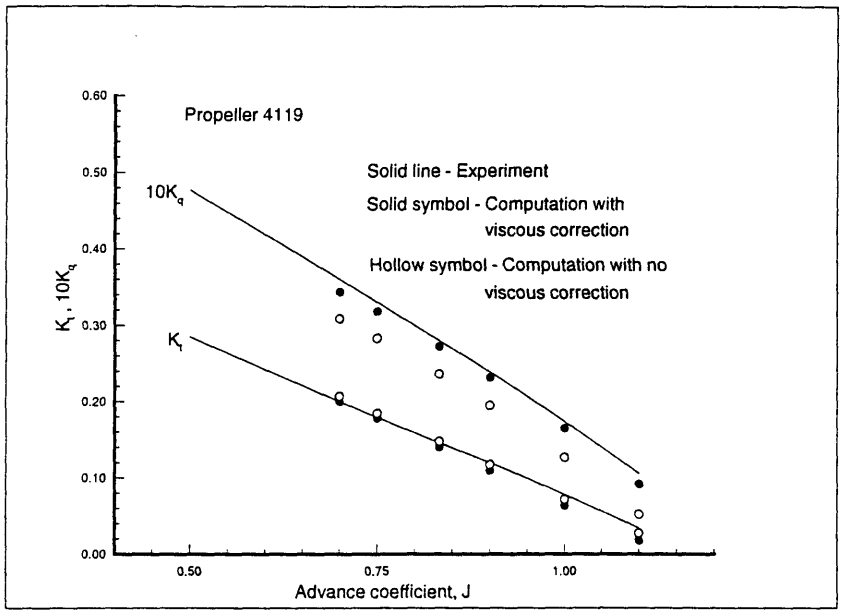

Fig. 2. Open Water Performance Curve, Propeller 4119 - Viscous Effect.

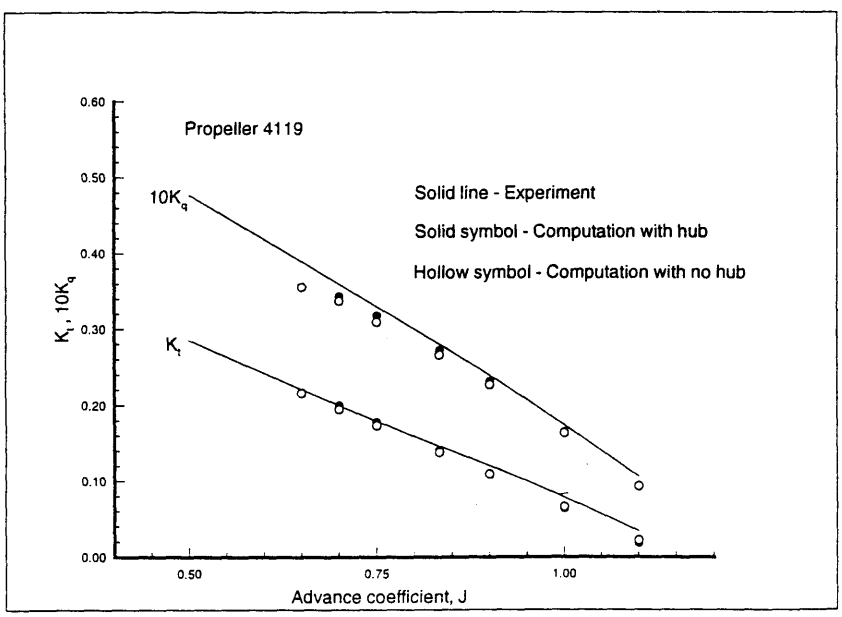

Fig. 3. Open Water Performance Curve, Propeller 4119 - Hub Effect.

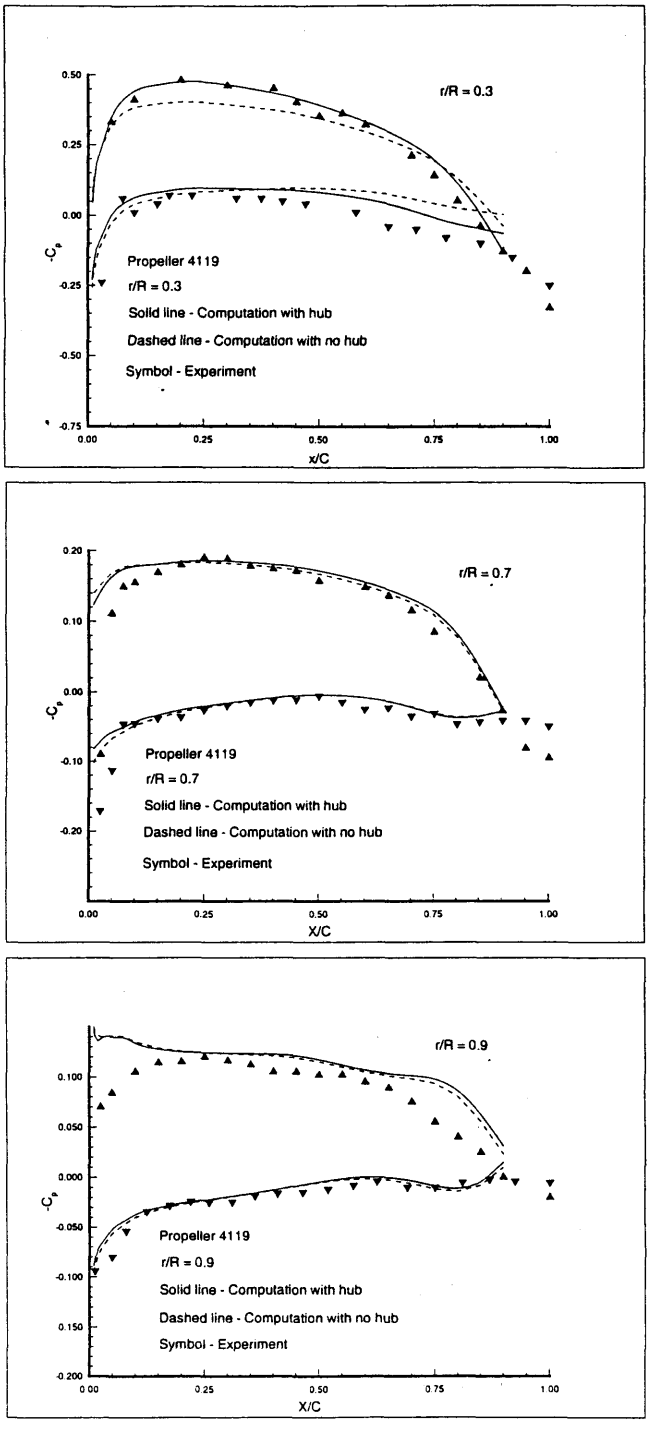

Fig. 4. Measured and Predicted Pressure Distribution on the Blade Surface of Propeller 4119.

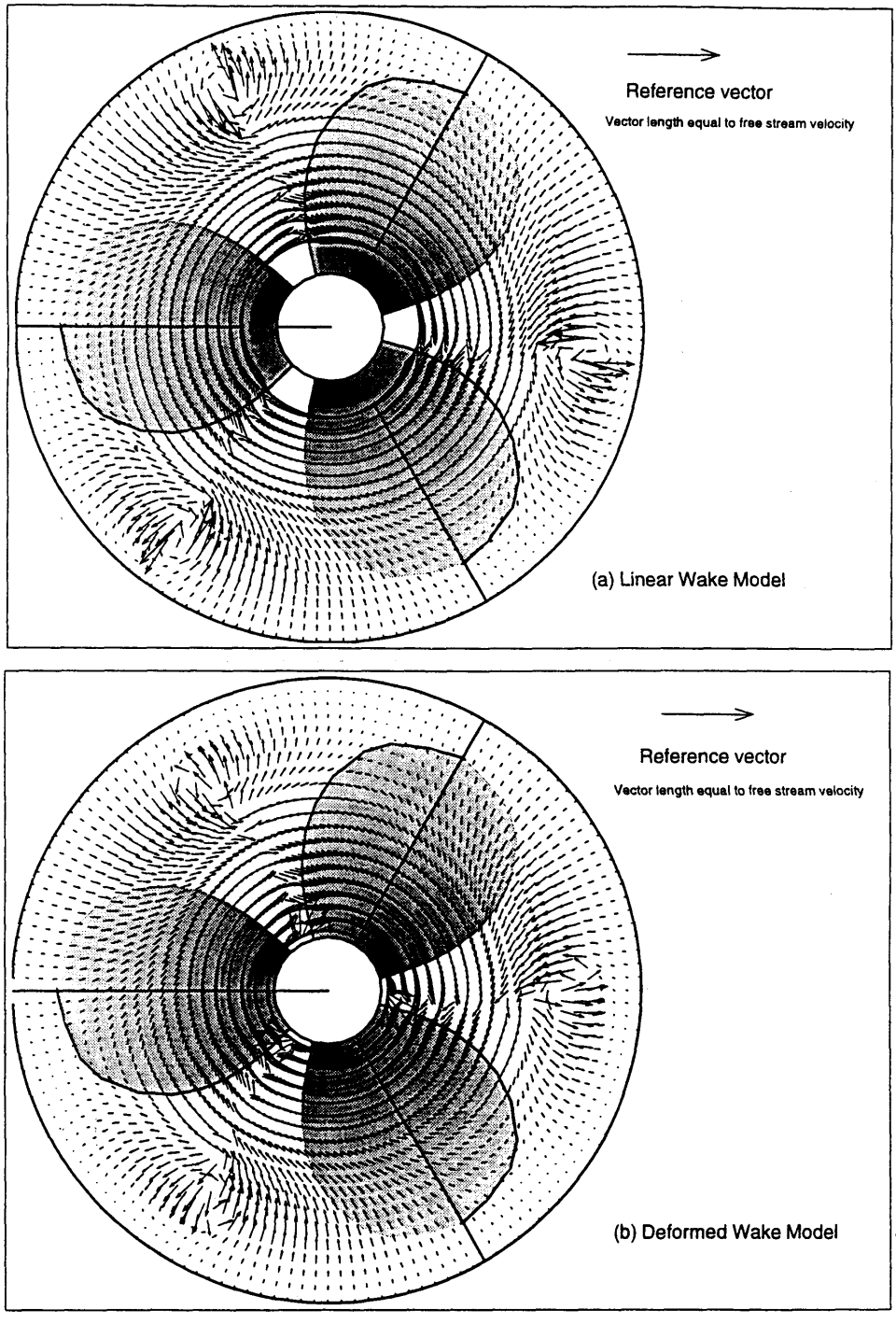

Fig. 5. Predicted Cross Flow Velocity Vectors on a Plane Behind Propeller 4119.

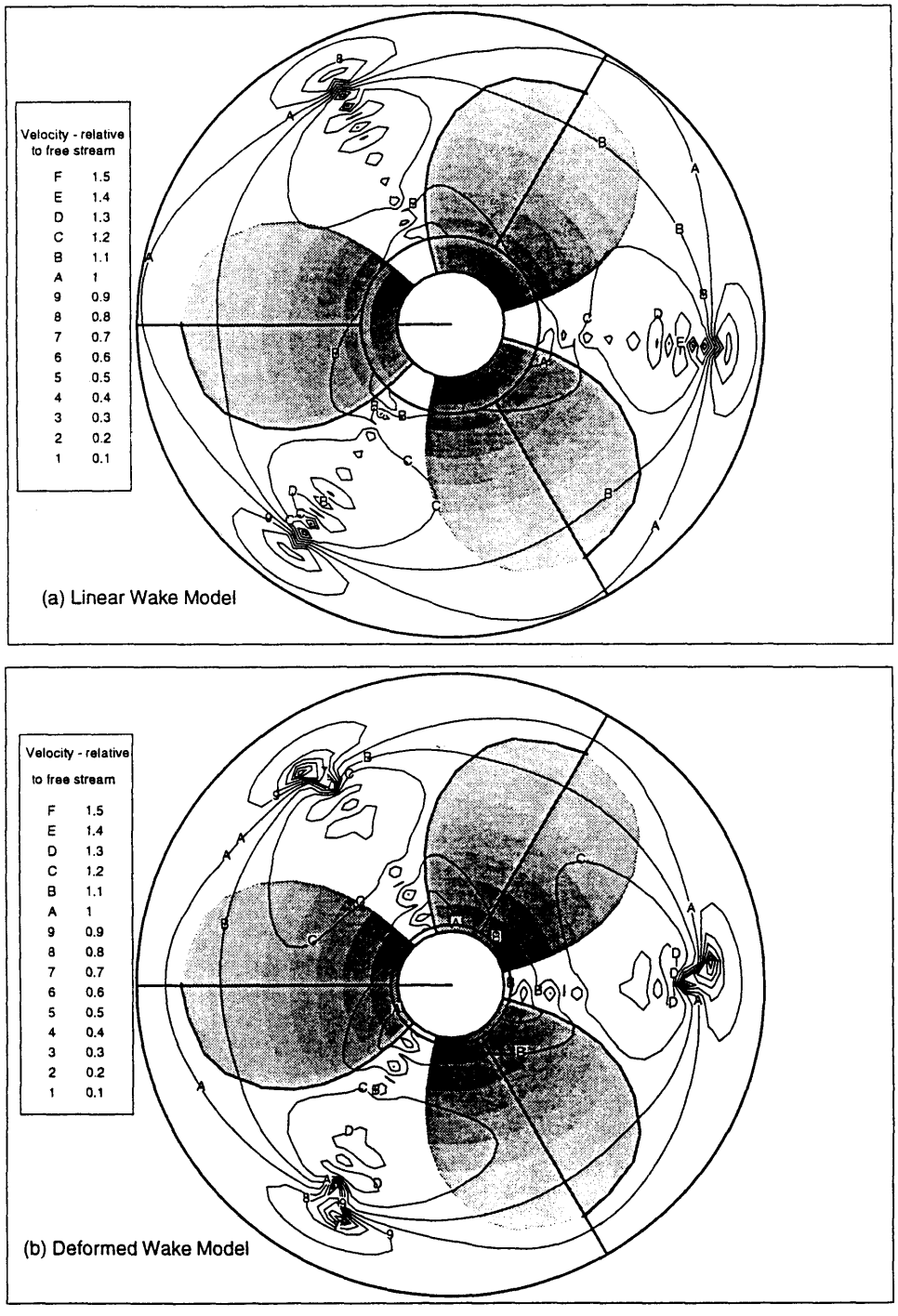

Fig. 6. Predicted Axial Velocity contour on a Plane behind Propeller 4119.

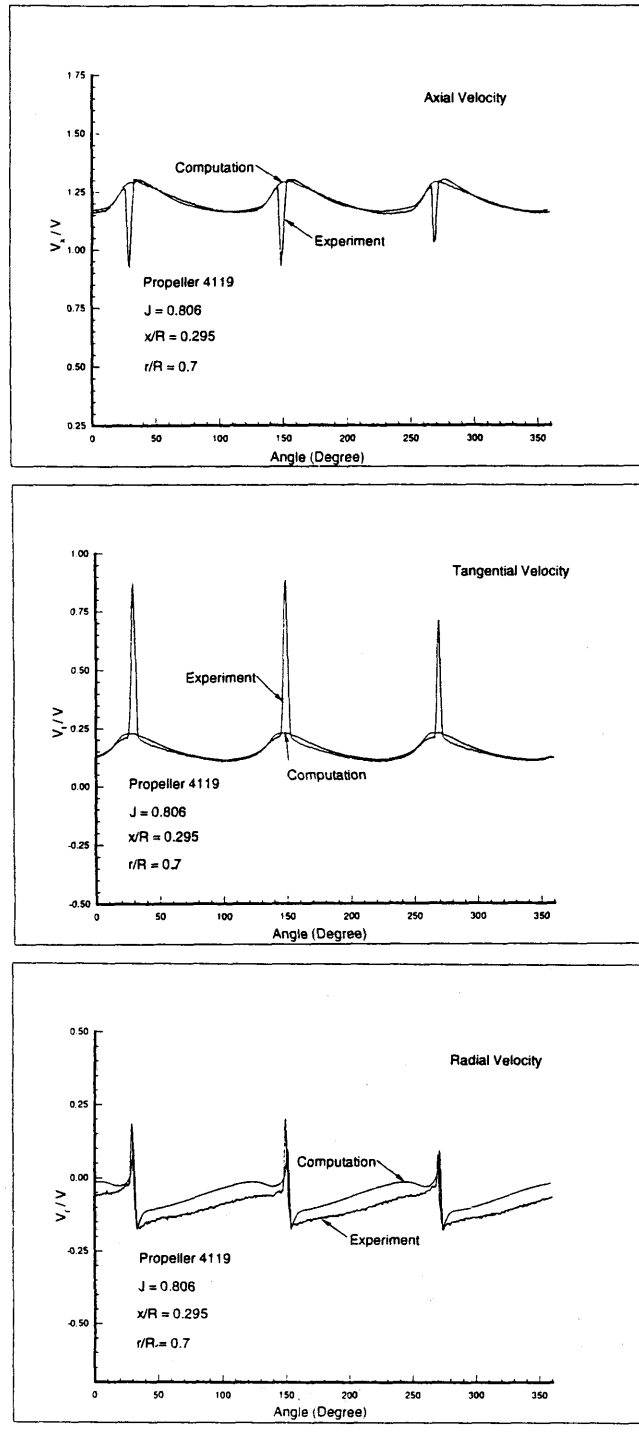

Fig. 7. Measured and Predicted Velocity Components Behind Propeller 4119.

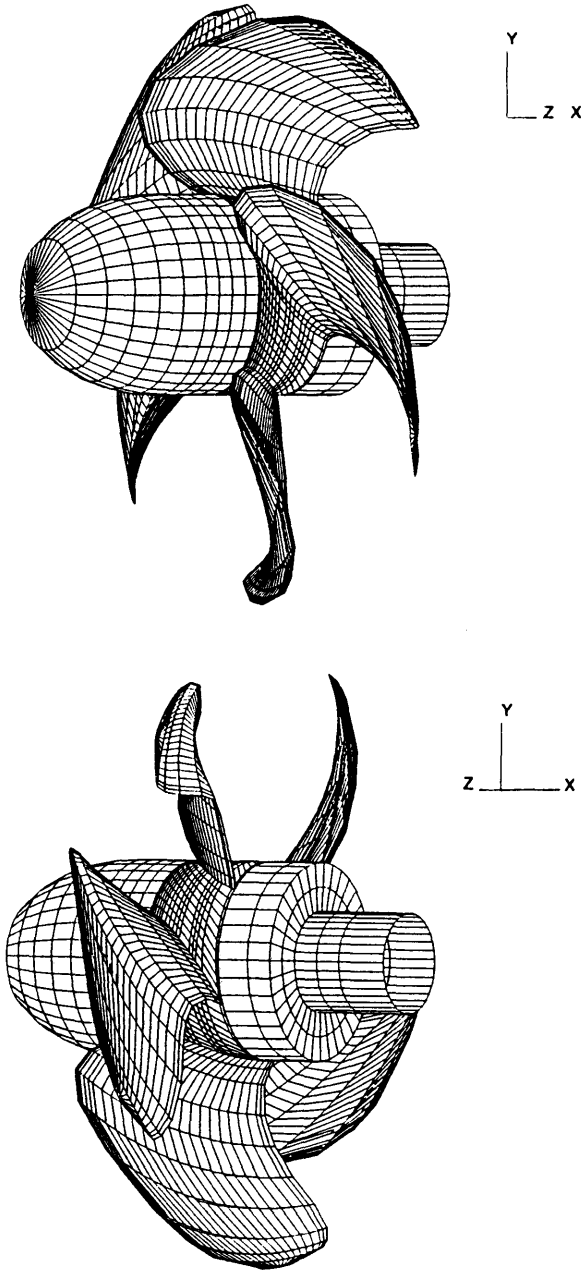

Fig. 8. Perspective Views of Discretized Propeller 4842.

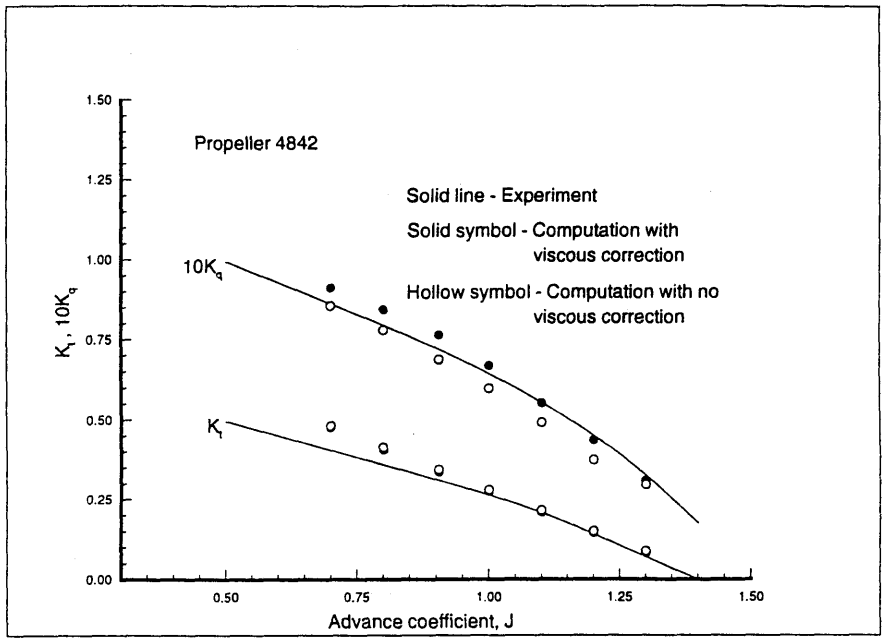

Fig. 9. Open Water Performance Curve, Propeller 4842 - Viscous Effect.

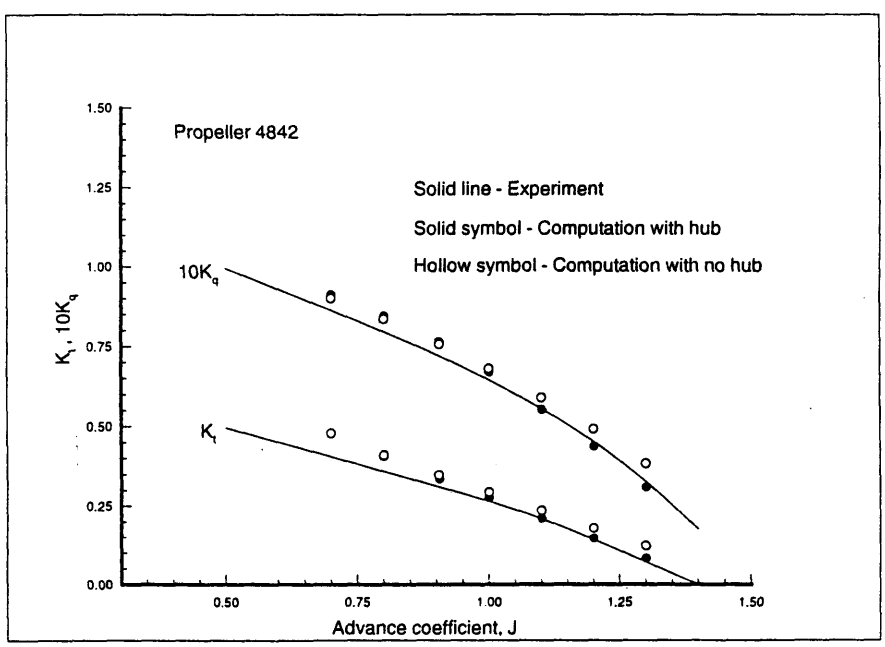

Fig. 10. Open Water Performance Curve, Propeller 4842 - Hub Effect.

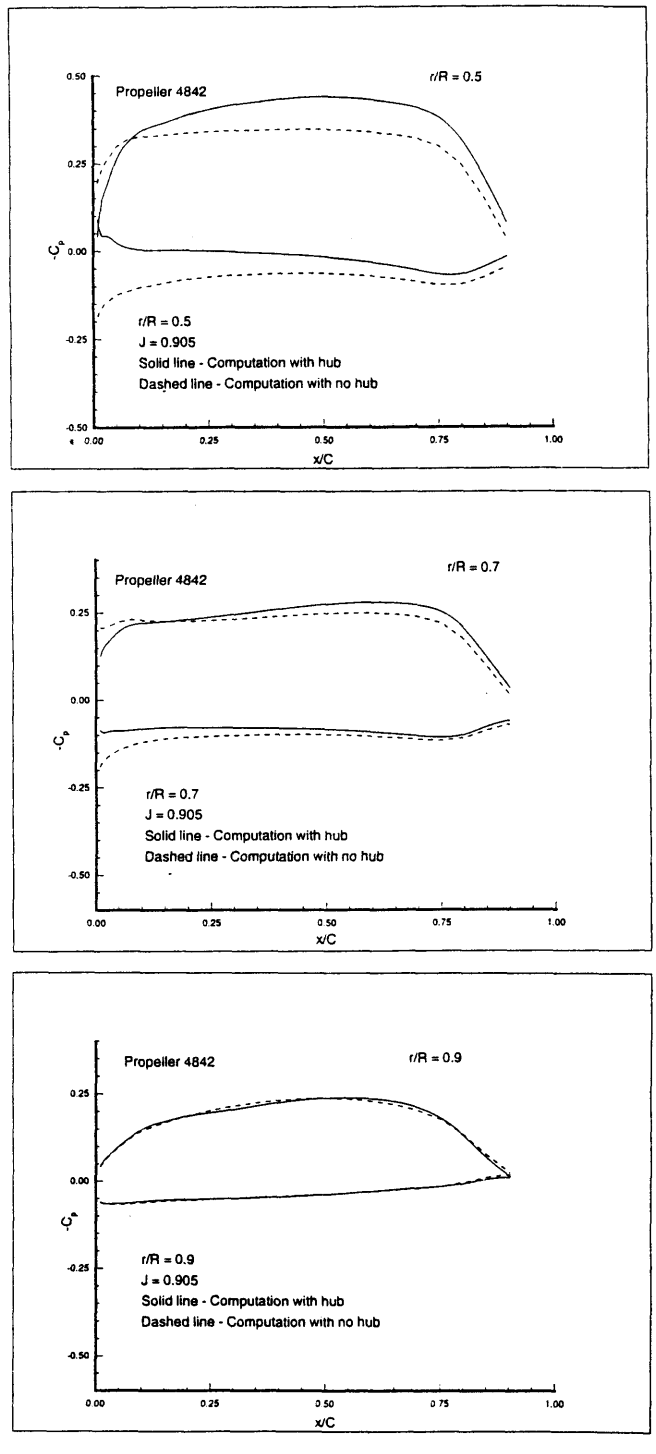

Fig. 11. Predicted Pressure Distribution on the Blade Surface of Propeller 4842.

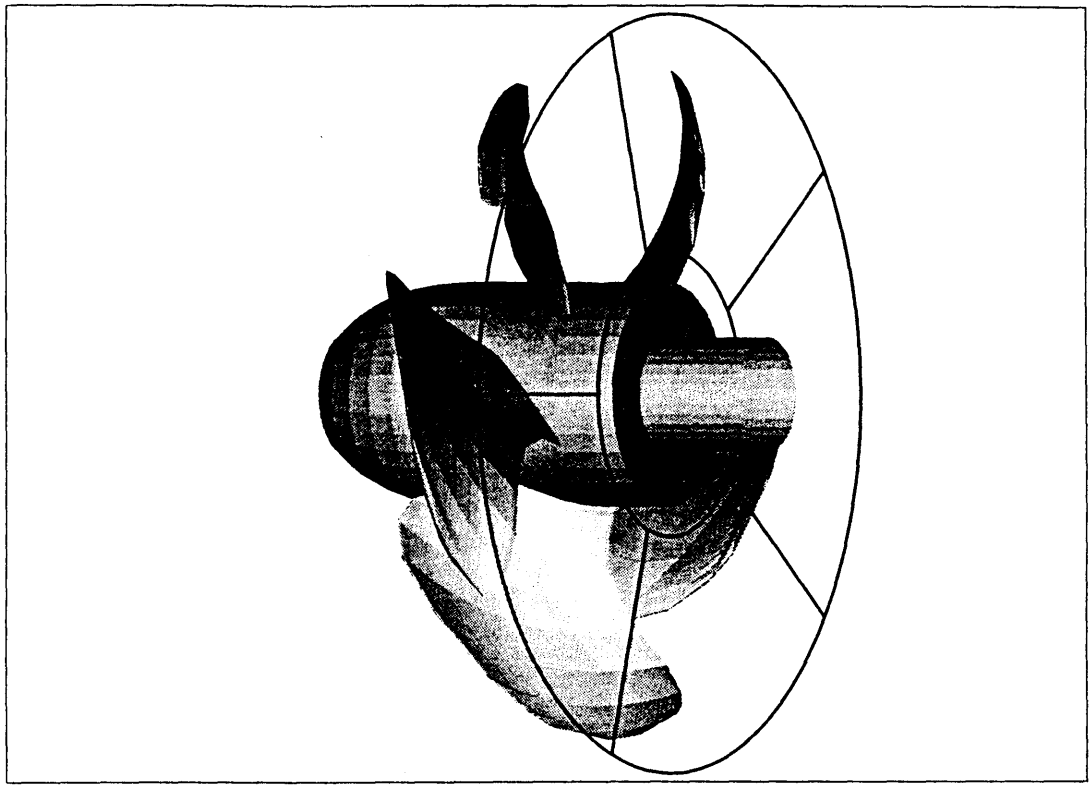

Fig. 12. Location of Velocity Measuring Plane with respect to the Propeller Blades, Propeller 4842

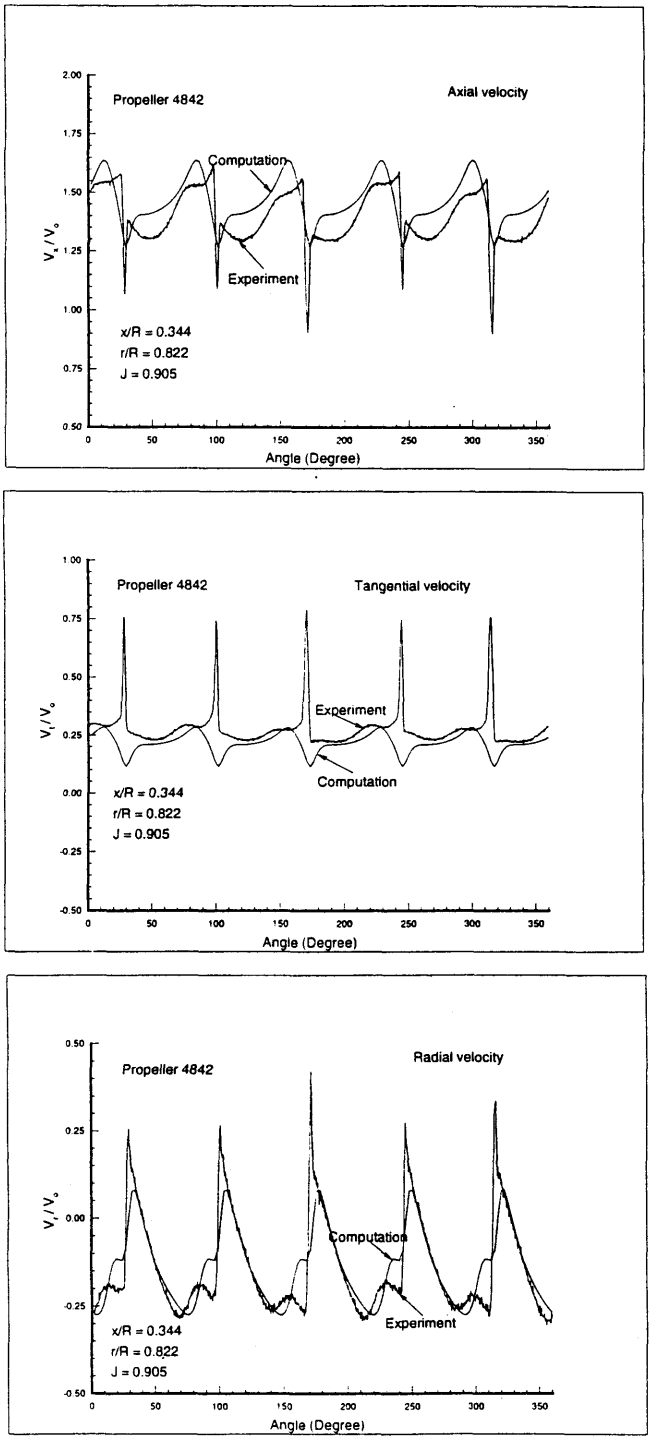

Fig. 13. Measured and Predicted Velocity Components Behind Propeller 4842.

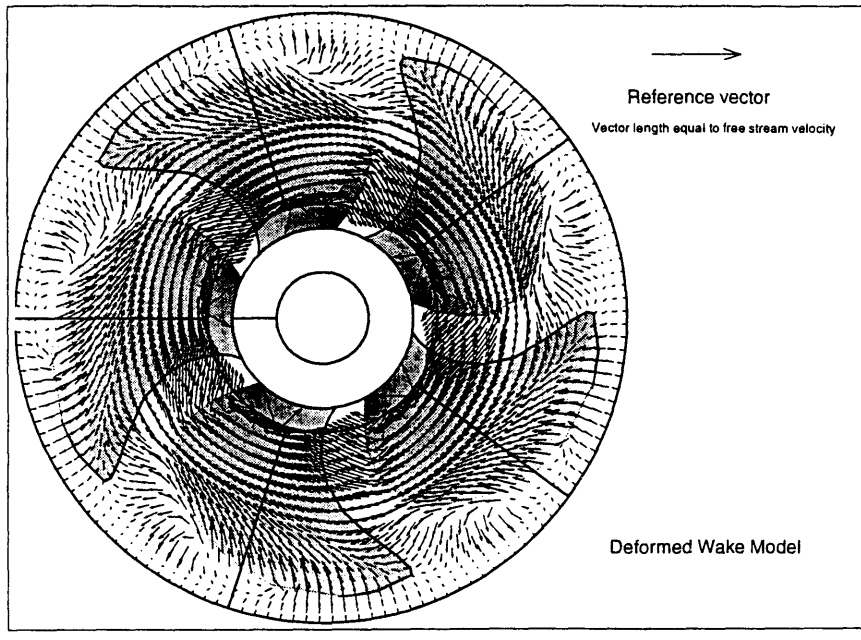

Fig. 14. Predicted Cross Flow Velocity Vectors on a Plane Behind Propeller 4842.

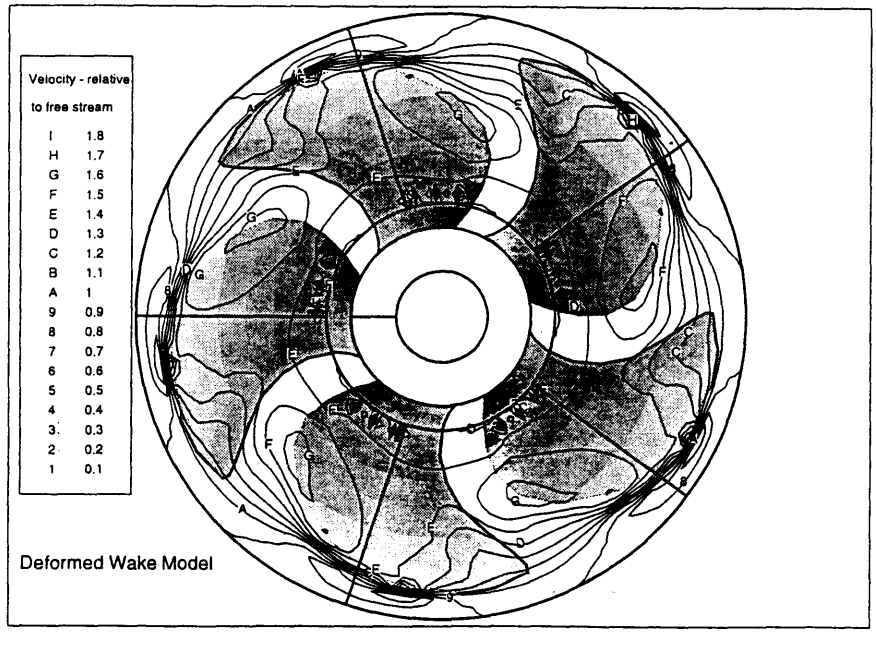

Fig. 15. Predicted Axial Velocity Contour on a Plane Behind Propeller 4842.

APPENDIX C

Calculations by MIT

Steady Performance Analysis for Two Propellers using MIT-PSF-10 prepared for 20^{th} ITTC Propulsor Committee Comparative Calculation of Propellers by Surface Panel Methods

Ching-Yeh Hsin and Justin E. Kerwin
Massachusetts Institute of Technology
Department of Ocean Engineering

July 17, 1992

1 Calculation Results

1.1 Standard-Condition Runs

We will first show the results of the "standard calculation conditions". In Table 1, the results of conditions required by ITTC are tabulated. All the calculations include the potential flow solutions and potential solutions with viscous corrections.

Viscous effects in MIT-PSF-10 are accounted for by a leading edge suction force correction and by the simple addition of tangential stresses derived from a constant frictional drag coefficient. The leading edge suction force correction is based on Polhamus' "leading edge suction analogy" [7], and the detail numerical implementation can been seen in [3]. In the following cases, the frictional drag coefficient is selected as $C_D = D/(\frac{1}{2}\rho V^2 c) = 0.007$, where D is the frictional drag/unit radius, V is the resultant inflow velocity at that radius and c is the expanded chord length.

The devised wake model of MIT-PSF-10 is based on MIT-PSF-2 wake model [1]. In the following cases, the contraction angle of the wake is 30°, and the ultimate tip wake radius is 0.83. The wake induced velocities calculated from MIT-PSF-2 are then used to generate the wake geometries.

The "recommended paneling" is 40 panels chordwise, and 30 panels spanwise. The "reference paneling" results are listed in Table 2. We have both increased and decreased the number of panels to check the convergence. In Table 2, all the results are without the viscous correction, and without the hub. The wake geometry is linear. The symbol $40c \cdot 30s$ indicates the number of panels used is 40 panels chordwise, and 30 panels spanwise.

The results of propeller 4119 at $J = 1.100$ are tabulated in Table 3, and the results of propeller 4842 at $J = 0.905$ are tabulated in Table 4. The calculated results of the propeller 4842 with the wrong rake (originally provided by ITTC) are also included in Table 5.

1.2 Complete runs of Propellers 4119 and 4842

We then calculated the forces of propellers 4119 and 4842 at different advance coefficients. All these calculations used the hub model suggested by ITTC (having fairwaters at both

ends), and used the devised wake model. Viscous corrections are included, and the frictional drag coefficient is selected as 0.007. The number of panels of all the runs is 40 panels chordwise, 30 panels spanwise.

This panel arrangement is illustrated in figures 1 and 2 for the two propellers. These figures also include grey-scale contour of the computed pressure distribution at the design advance coefficient.

Results are first tabulated in Table 6 and Table 7, and then plotted against experimental results in Figure 3 and Figure 4.

1.3 Effect of the Hub Geometries

To understand the effect of the hub geometries, we have calculated the forces on propeller 4119 by using three different hub geometries, along with the no hub results. Besides the hub model suggested by ITTC, we also used hub geometries with constant radii downstream and upstream. This is to simulate the real experiments which the propellers may be driven either from upstream, or from downstream. We named the ITTC hub model as the *hub model 1*, the hub which has a fairwater downstream, and constant radius upstream as the *hub model 2* (driven from upstream), and the hub which has a fairwater upstream, and constant radius downstream as the *hub model 3* (driven from downstream). Figure 5 shows these three different hub models. The calculated forces with hub model 1 have been shown in Table 6, the calculated forces with hub model 2 are shown in Table 8, and the calculated forces with hub model 3 are shown in Table 9. The results without hub are shown in Table 10. We have also plotted theses results against the experimental data in Figure 6.

It should be noted that a singularity will exist at the aft end of a closed hub unless the blade circulation is zero at the hub radius. This can be avoided by introducing a finite core radius to the hub vortex. PSF-10 has a provision for specifying a core radius, and hub forces are then computed assuming constant pressure on all panels that fall within the core. The results for propeller 4119 are shown in Table 11 by using the different core sizes. All the calculations listed before used a core radius of 10% of the hub radius.

2 Comparison with lifting surface methods

The [1] presented panel method is expected to be more accurate than any lifting surface method (linearized about the mean camber surface). The largest differences between the two methods will occur locally, namely at the edges of the blade where the lifting surface assumptions are not valid. However, in some cases (especially for thickness to chord ratios larger than 10%) even the global solutions from the two methods may differ. For example, this may be seen in Figure 7 where the circulation distributions are shown as predicted from the panel method (thick solid line) and from a conventional lifting surface method [1] (thin solid line). The lifting surface theory models the thickness with sources distributed on the mean camber surface. Thus, the effects of the thickness sources on one blade due to the other blades as well as due to the twist of the blade itself are readily included in the solution. However, the thickness/loading coupling, which is present even in the case of the planar wings, is not

[1] The present section has been prepared by Sangwoo Pyo and Spyros Kinnas.

included. A way of including this coupling has been developed recently [5]. The circulation distribution when the thickness/loading coupling is included is also shown in Figure 7 (circles). The agreement with the circulation distribution from the panel method is remarkable. The improved lifting surface method however, is still expected to fail at the blade edge.

3 Method of Calculation

MIT-PSF-10 is a lower order, potential based panel method. It uses hyperboloidal panel geometries and imposes the boundary condition on the panel centroid. The detail of the theory and numerical schemes can be found in [4], [6], [3] and [2].

References

[1] D.S. Greeley and J.E. Kerwin. Numerical methods for propeller design and analysis in steady flow. *Trans. SNAME*, vol 90, 1982.

[2] C-Y. Hsin, J.E. Kerwin, and S.A. Kinnas. A panel method for the analysis of the flow around highly skewed propellers. In *Proceedings of the Propellers/Shafting '91 Symposium*, pages 1–13 (paper No. 11), Virginia Beach, VA, September 1991. Soc. Naval Arch. & Marine Engnrs.

[3] Ching-Yeh Hsin. *Development and Analysis of Panel Method for Propellers in Unsteady Flow*. PhD thesis, Department of Ocean Engineering, MIT, September 1990.

[4] J.E. Kerwin, S.A. Kinnas, J-T Lee, and W-Z Shih. A surface panel method for the hydrodynamic analysis of ducted propellers. *Trans. SNAME*, 95, 1987.

[5] S.A. Kinnas. A general theory for the coupling between thickness and loading for wings and propellers. *Journal of Ship Research*, 36(1):pp. 59–68, March 1992.

[6] Jin-Tae Lee. *A Potential Based Panel Method for the Analysis of Marine Propellers in Steady Flow*. PhD thesis, MIT, Department of Ocean Engineering, 1987.

[7] Edward C. Polhamus. A concept of the vortex lift of sharp-edge delta wings based on a leading-edge-suction analogy. Technical Report NASA TN D-3767, Langley Research Center, 1966.

Without Viscous Correction

paneling	hub	wake	KT	KQ	η
recommended	w/o	linear	0.145	0.0237	0.813
reference	w/o	linear	see	next	table
recommended	w/	linear	0.143	0.0241	0.784
recommended	w/o	devised	0.151	0.0242	0.828
recommended	w/	devised	0.148	0.0243	0.805

With Viscous Correction

paneling	hub	wake	KT	KQ	η
recommended	w/o	linear	0.142	0.0259	0.725
reference	w/o	linear	see	next	table
recommended	w/	linear	0.138	0.0263	0.698
recommended	w/o	devised	0.147	0.0265	0.737
recommended	w/	devised	0.144	0.0266	0.716

Table 1: Propeller 4119, J=0.833

paneling	KT	KQ	η
$20c \cdot 10s$	0.152	0.0245	0.823
$40c \cdot 20s$	0.148	0.0241	0.812
$40c \cdot 30s$	0.145	0.0237	0.813
$60c \cdot 30s$	0.147	0.0241	0.808
$60c \cdot 40s$	0.145	0.0238	0.809
$80c \cdot 30s$	0.147	0.0242	0.806
$80c \cdot 40s$	0.146	0.0240	0.807

Table 2: Propeller 4119 Convergence Test (J=0.833)

Without Viscous Correction

paneling	hub	wake	KT	KQ	η
recommended	w/o	linear	0.0393	0.00734	0.938
recommended	w/o	devised	0.0398	0.00744	0.937

With Viscous Correction

paneling	hub	wake	KT	KQ	η
recommended	w/o	linear	0.0350	0.00890	0.689
recommended	w/o	devised	0.0355	0.00900	0.690

Table 3: Propeller 4119, J=1.100

Without Viscous Correction

paneling	hub	wake	KT	KQ	η
recommended	w/	devised	0.315	0.0653	0.693

With Viscous Correction

paneling	hub	wake	KT	KQ	η
recommended	w/	devised	0.306	0.0693	0.637

Table 4: Propeller 4842, J=0.905

Without Viscous Correction

paneling	hub	wake	KT	KQ	η
recommended	w/	devised	0.294	0.0593	0.714

With Viscous Correction

paneling	hub	wake	KT	KQ	η
recommended	w/	devised	0.285	0.0634	0.648

Table 5: Propeller 4842 with wrong rake, J=0.905

J	KT	KQ	η
0.500	0.282	0.0465	0.483
0.700	0.201	0.0354	0.633
0.833	0.144	0.0266	0.716
0.900	0.114	0.0221	0.740
1.100	0.024	0.0073	0.586

Table 6: Propeller 4119 with ITTC hub (hub model 1)

J	KT	KQ	η
0.500	0.530	0.1032	0.408
0.700	0.406	0.0872	0.518
0.905	0.306	0.0693	0.637
1.100	0.202	0.0509	0.695
1.300	0.084	0.0287	0.609

Table 7: Propeller 4842 with ITTC hub (hub model 1)

J	KT	KQ	η
0.500	0.282	0.0467	0.481
0.700	0.202	0.0358	0.630
0.833	0.146	0.0267	0.727
0.900	0.117	0.0226	0.739
1.100	0.028	0.0080	0.624

Table 8: Propeller 4119 with hub model 2

J	KT	KQ	η
0.500	0.296	0.0469	0.503
0.700	0.211	0.0361	0.652
0.833	0.151	0.0274	0.729
0.900	0.121	0.0230	0.753
1.100	0.031	0.0084	0.638

Table 9: Propeller 4119 with hub model 3

J	KT	KQ	η
0.500	0.273	0.0424	0.513
0.700	0.201	0.0338	0.661
0.833	0.147	0.0265	0.737
0.900	0.120	0.0225	0.765
1.100	0.035	0.0089	0.689

Table 10: Propeller 4119 without hub

core radius	KT	KQ
0.00	0.142	0.0266
0.02 (10%)	0.144	0.0266
0.04 (20%)	0.144	0.0266

Table 11: The results for propeller 4119 by using the different hub vortex core radius

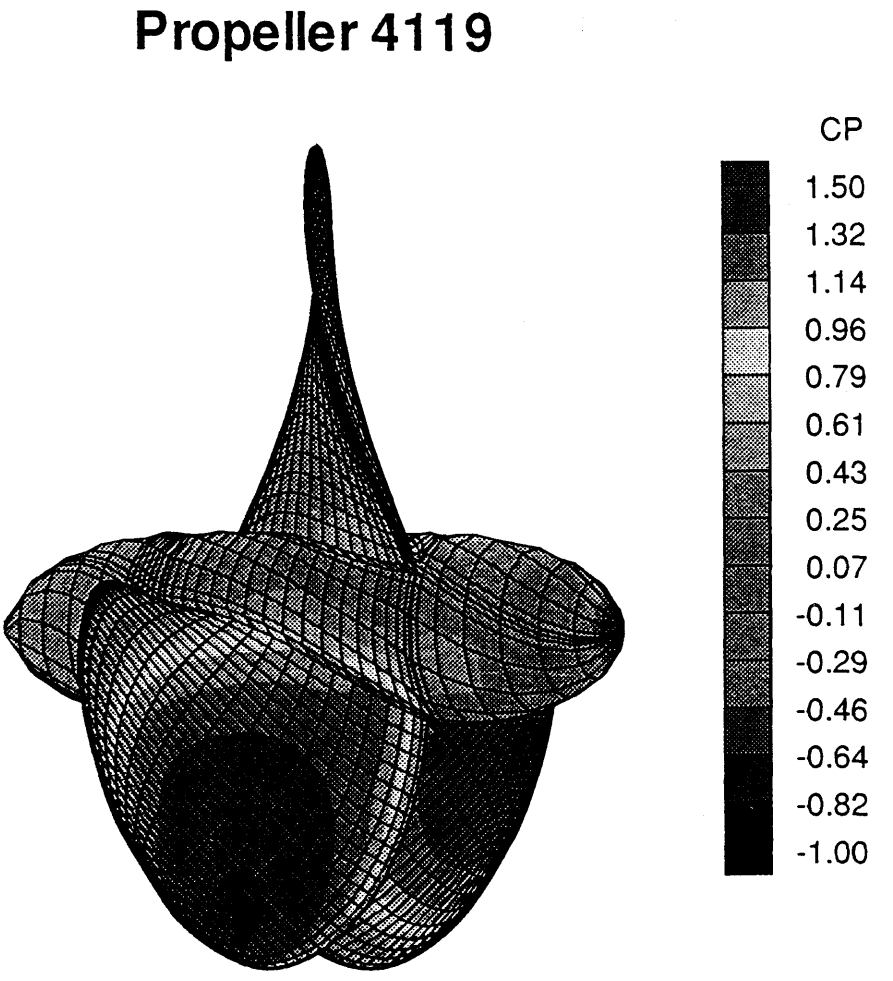

Figure 1: The panel arrangement and pressure distribution on propeller 4119 at the design advance coefficient. The paneling used here is the recommended paneling (40 panels chordwise, 30 panels spanwise).

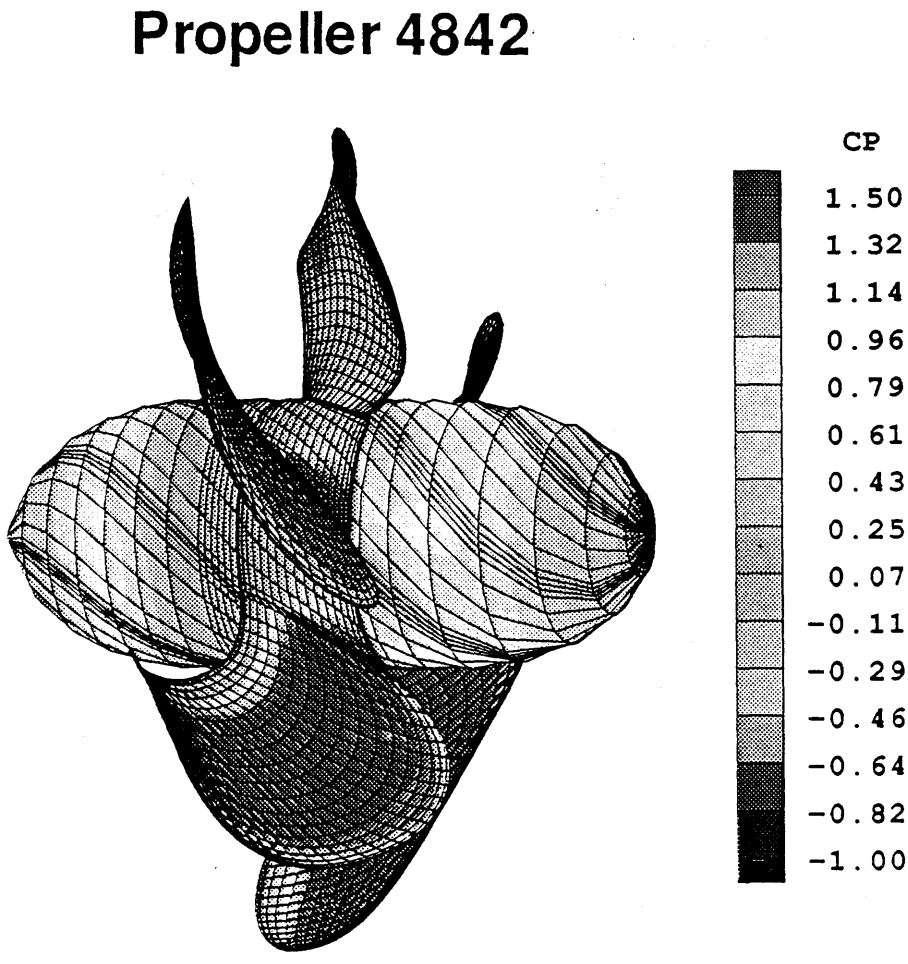

Figure 2: The panel arrangement and pressure distribution on propeller 4842 at the design advance coefficient. The paneling used here is the recommended paneling (40 panels chordwise, 30 panels spanwise).

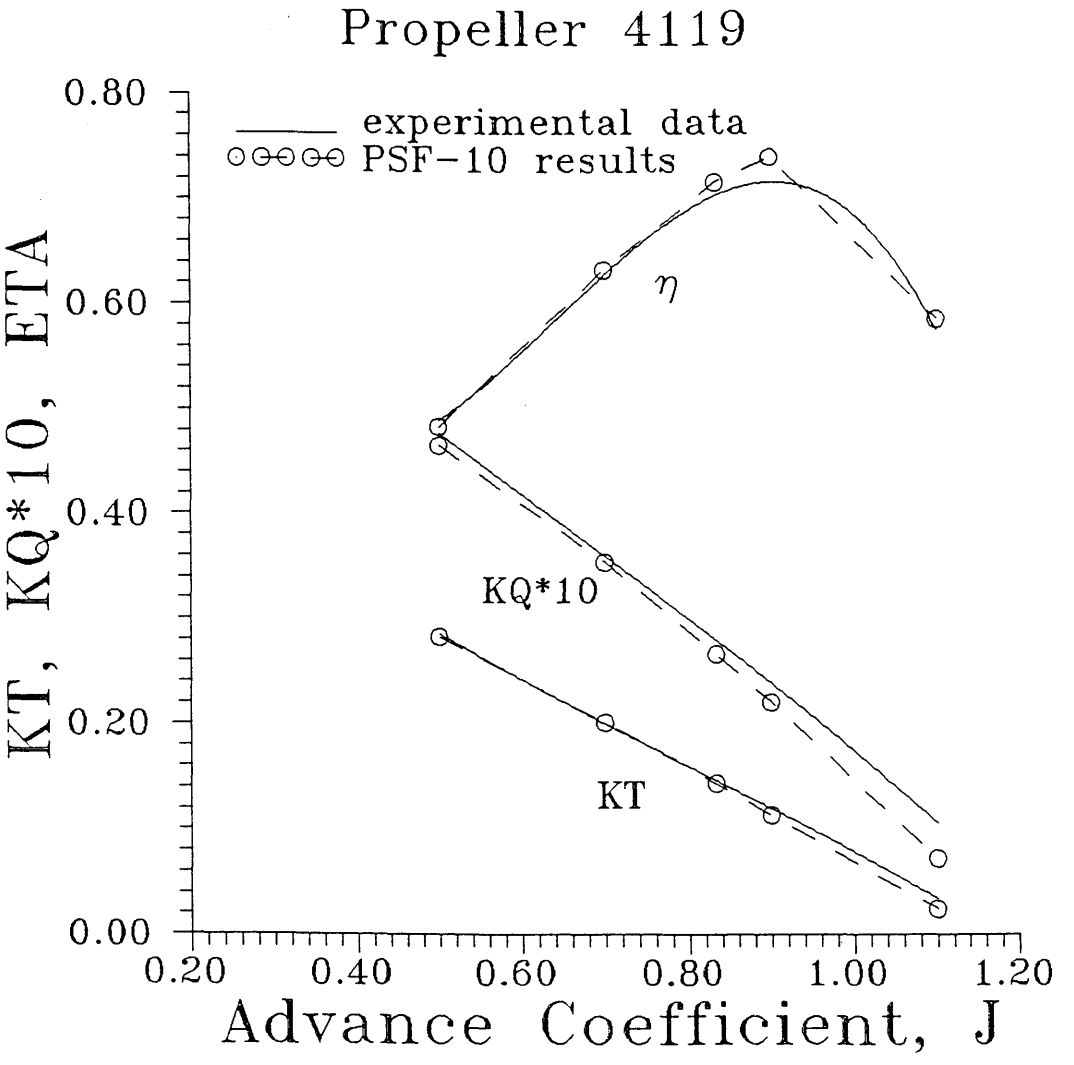

Figure 3: Computational results vs. experimental data of propeller 4119. All the computational results used ITTC hub model, and a drag coefficient 0.007.

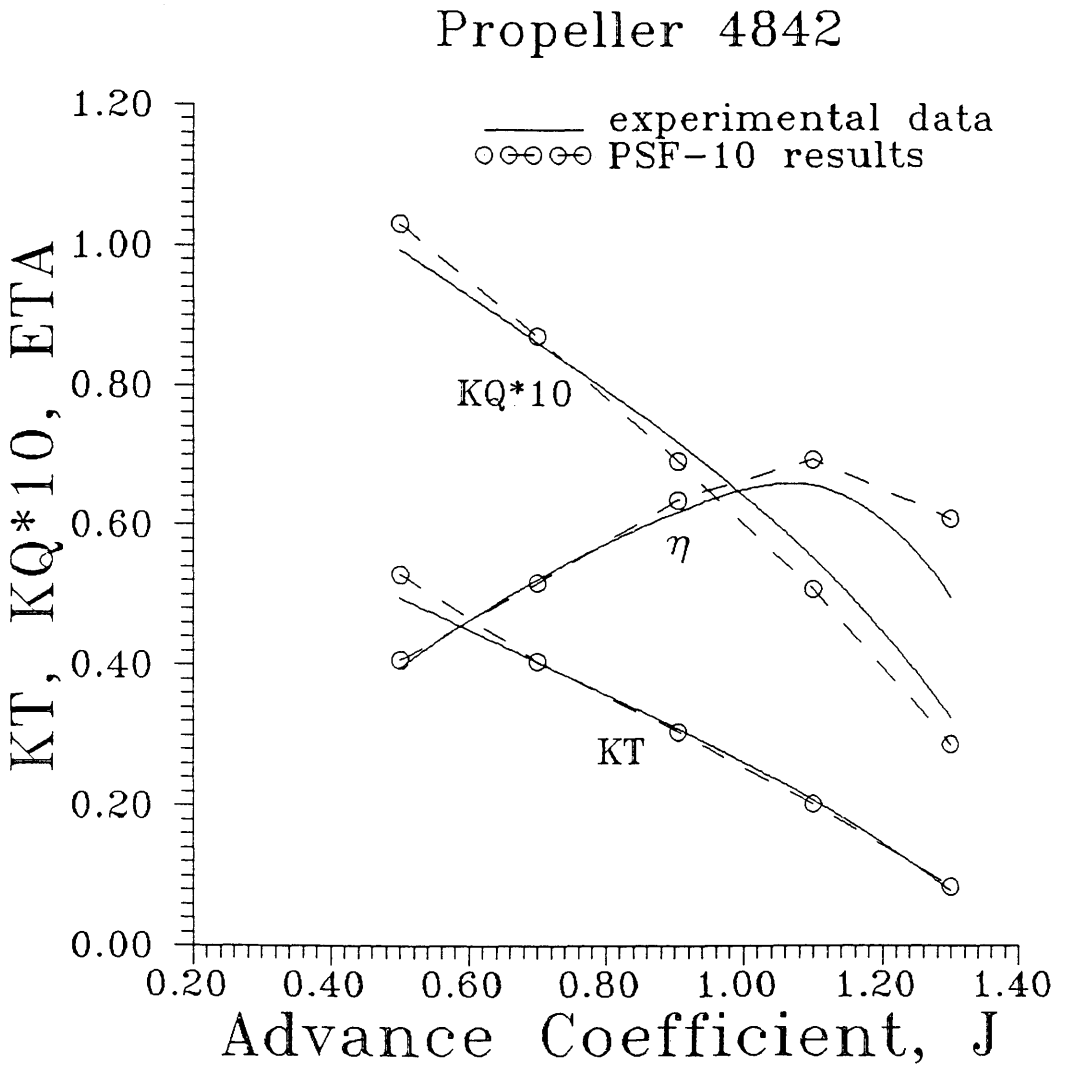

Figure 4: Computational results vs. experimental data of propeller 4842. All the computational results used ITTC hub model, and a frictional drag coefficient 0.007.

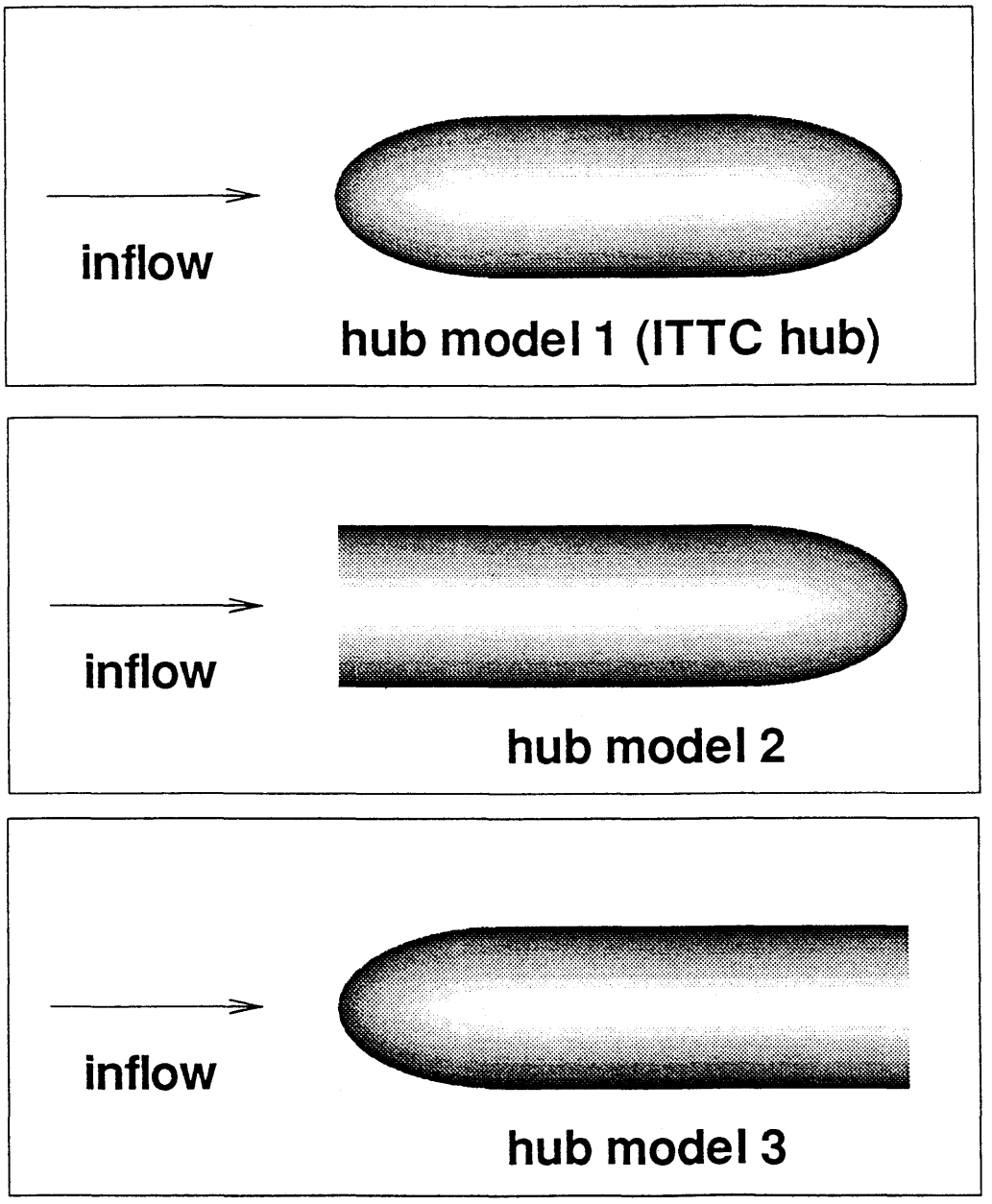

Figure 5: Different hub models used to investigate the hub effect.

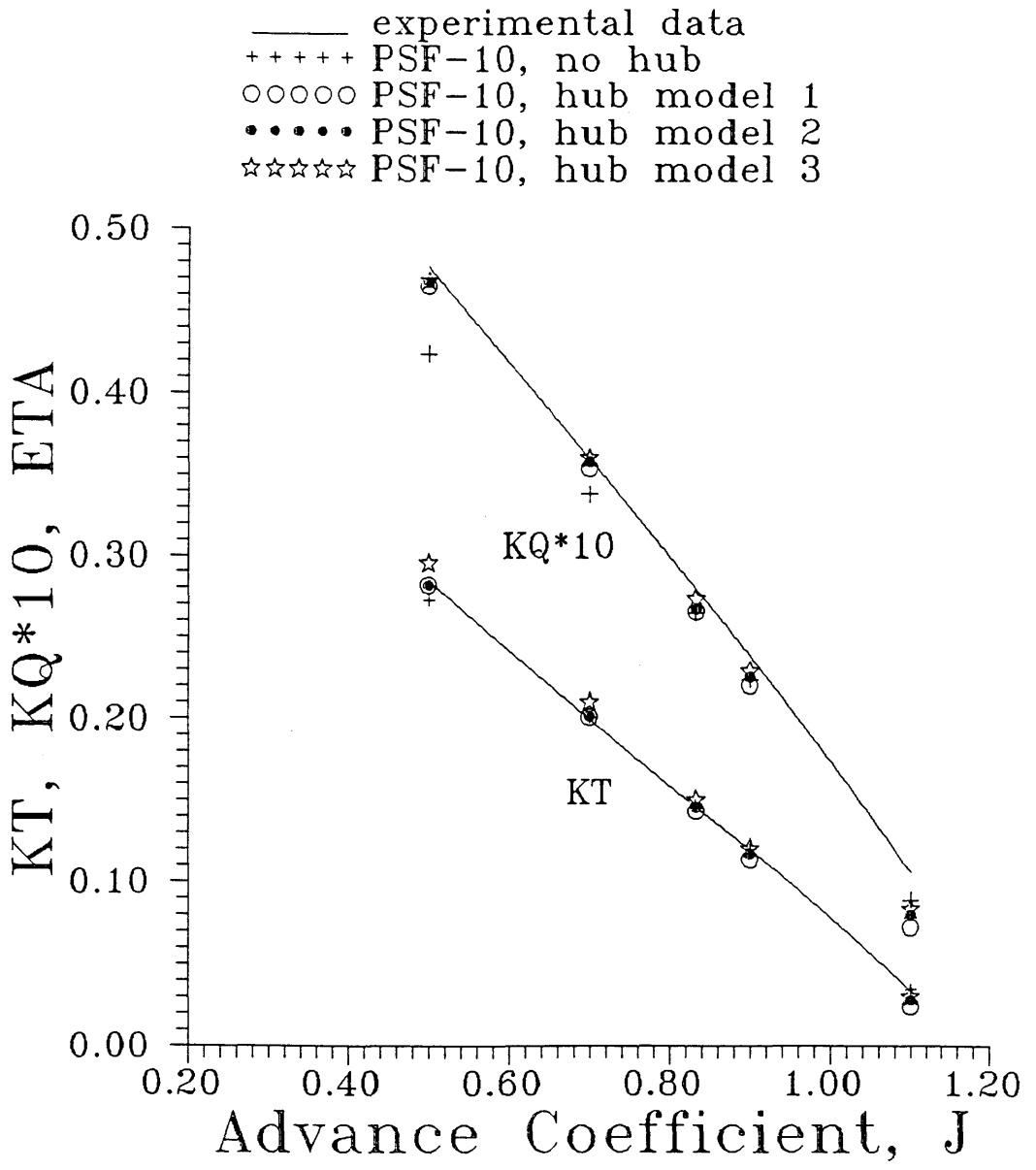

Figure 6: Computation results of different hub models of propeller 4119.

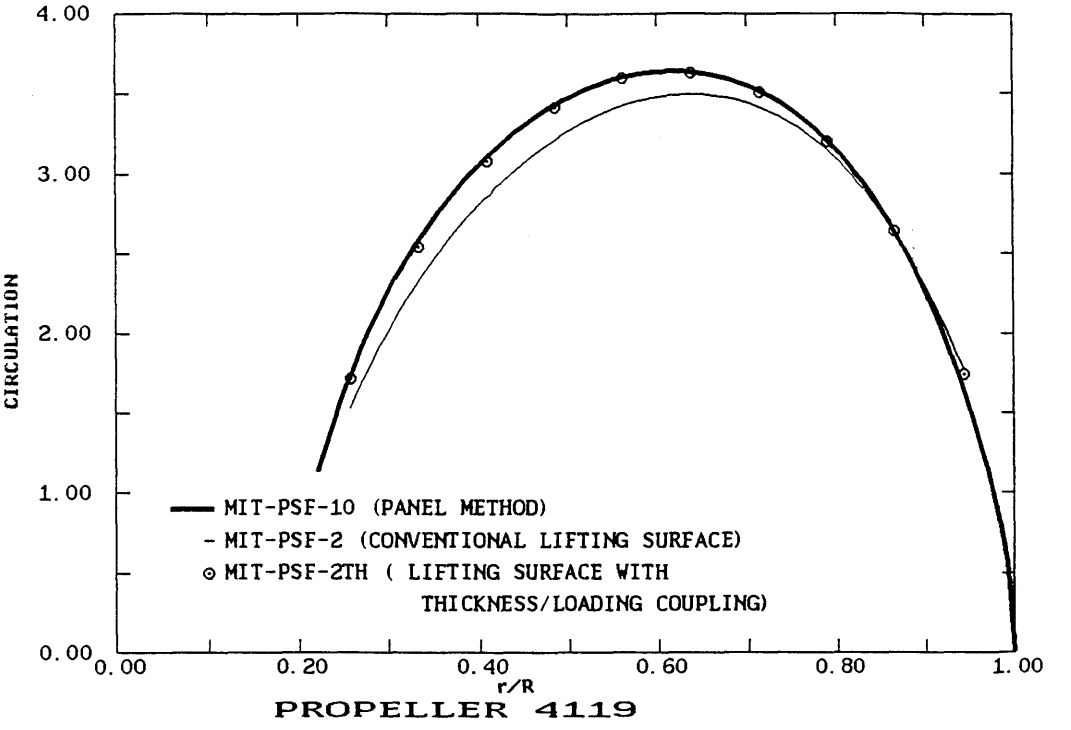

Figure 7: Circulation distribution (made non-dimensional on $2\pi RV_S$, where R is the radius of propeller, and V_S is the ship speed) for the 4119 propeller predicted from different methods (the effect of hub is not included).

APPENDIX D

Calculations by AMI

Calculations for the DTRC 4119 and DTRC 4842 Propellers Using VSAERO/MPROP and USAERO Panel Codes

Prepared by:

Analytical Methods

B. Maskew, J.S. Fraser, J.B. Murray and M.J. Summa

Prepared for the 20th ITTC Propulsor Committee Workshop

Korea, August 1992

July 31, 1992

Introduction

Analytical Methods, Inc. (AMI) analyzed the two workshop propeller configurations, DTRC 4119 and DTRC 4842, using the VSAERO/MPROP and USAERO panel codes. VSAERO/ MPROP is a Marine Propeller version of AMI's widely used VSAERO program, the MPROP extension providing certain features for propeller applications in steady axisymmetric conditions. USAERO is a time-stepping panel code with a very general capability. Although it was developed primarily for aircraft maneuver and store release calculations, its general options for multiple moving frames of reference allow a very broad scope of application covering complete vehicles, helicopter, automobiles, trains, ships, etc. Even though no specific development has been undertaken for marine propeller applications, the general capability of USAERO allows such configurations to be treated, and in fact, a propeller in non-uniform flow, a counter-rotating propulsor, a propeller with cyclical pitch variation and a propeller near a free surface, have been briefly studied. USAERO was, therefore, included in the current study, the time-stepping calculations proceeding until essentially steady state conditions were reached.

The wake models used in the present calculations were different; the VSAERO cases used a simple helical wake with the pitch determined by the local advance coefficient. In the USAERO calculations, a new set of wake panels is created along the shedding lines at each time step, and all the existing wake panels are convected with the local flow for the duration of the time step. The calculations normally start impulsively from rest with no initial wake. With the present range of advance coefficients, the calculations reach essentially steady state conditions within about 20 steps. In the present axisymmetric flow conditions, the number of unknowns in USAERO can be reduced to the number of panels on a single blade (plus corresponding strips of panels along the hub, if present) using an "SSCOPY" option (for same solution copy) when generating the configuration geometry. A similar option, "RSCOPY" provides a "Repeat Solution" capability for treating the cyclical conditions encountered in non-uniform flows.

Both VSAERO/MPROP and USAERO include coupled integral boundary layer calculations, which provide the skin friction distribution over the surfaces as well as boundary layer displacement effect, which is modelled in the codes, using a transpiration technique. The VSAERO boundary layer coupling has been in use for over 12 years and has been extensively tested and refined. The USAERO unsteady boundary layer coupling has been in active use only over the past two years and is less robust in application; some minor problems occurred in the boundary layer displacement effect coupling with the panel boundary conditions in the present cases.

A brief outline of the method formulation and numerical procedure for the two codes is given in the following two sections before discussion of the actual calculations.

2.0 MATHEMATICAL MODEL

2.1 General

The mathematical foundation for VSAERO and USAERO are very similar. The mathematical models for the two codes are therefore outlined together here before discussing the numerical procedures in Section 3.

2.2 Basic Equations

Consider the *configuration* moving with velocity, $\vec{V}_B$, through an unbounded fluid initially at rest, Fig. 2.1. The basic assumptions are that the effects of viscosity are largely confined to thin boundary layers on the *configuration* surface and that wake vorticity is essentially concentrated in thin, free-shear layers and discrete vortex filaments. The majority of the flow is, therefore, regarded as inviscid, irrotational and incompressible. Laplace's equation can then be applied:

$$\nabla^2\phi = 0 \tag{2.1}$$

The convention adopted here is that the perturbation velocity is the *negative* gradient of ϕ:

$$\vec{v} = -\nabla\phi \tag{2.2}$$

Green's Theorem is applied next; note that with $\nabla^2\phi = 0$, the volume integral disappears. The flow is therefore uniquely determined by surface integrals of ϕ and its normal derivative over the surface of the *configuration* and its *wake*. Thus the velocity potential, ϕ_p, for a point, P, on the wetted side of the surface is

$$\phi_p = \frac{1}{4\pi}\iint_{S-P} \phi\,\vec{n}\cdot\nabla\left(\frac{1}{r}\right)dS + \frac{\phi_p}{2} - \frac{1}{4\pi}\iint_S \frac{1}{r}\vec{n}\cdot\nabla\phi\,dS + \frac{1}{4\pi}\iint_W (\phi_U - \phi_L)\,\vec{n}\cdot\nabla\left(\frac{1}{r}\right)dW \tag{2.3}$$

where $\vec{n}$ is the outward normal from the surface and r is the length of the vector from the surface element, dS, to the point, P. S-P signifies that the point, P, is excluded from the surface integral--the limiting process for the singular point when $r \to 0$ yields the local contribution, $\phi_p/2$.

The first integral in Eq. (2.3) is the contribution from a surface distribution of normal doublets of strength,

$$\mu = \frac{\phi}{4\pi} \tag{2.4}$$

The second integral is the contribution from a surface distribution of sources of strength,

$$\sigma = -\frac{\vec{n}\cdot\nabla\phi}{4\pi} \tag{2.5}$$